

## Synthesis and Characterization of Temperature Controlled SnO<sub>2</sub> Nanoparticles by Solid-state Reaction Method

Vijay Garg<sup>1,\*</sup>, Harsh Sharma<sup>1</sup>, Divya Rehani<sup>2,3</sup>, Renu Kumari<sup>2,4</sup>, Vipin Kumar<sup>4</sup>,  
Manoj Kumar Tiwari<sup>5</sup>, Shailesh Narain Sharma<sup>3,6</sup>, Manish Saxena<sup>7</sup>

<sup>1</sup> Department of Physics, M.M. College Modinagar, 201204 Ghaziabad (U.P.), India

<sup>2</sup> Dr. A.P.J. Abdul Kalam Technical University, 226031 Lucknow (U.P.), India

<sup>3</sup> Council of Scientific & Industrial Research-National Physical Laboratory, 110012 New Delhi, India

<sup>4</sup> Department of Physics, KIET Group of Institutions, 201206 Ghaziabad (U.P.), India

<sup>5</sup> Department of Electronics, Bhaskaracharya College of Applied Science, Delhi University,  
110075 Delhi, India

<sup>6</sup> Academy of Scientific and Innovative Research ACSIR, 201002 Ghaziabad (U.P.), India

<sup>7</sup> Moradabad Institute of Technology, 244001 Moradabad, India

(Received 14 April 2020; revised manuscript received 20 August 2020; published online 25 August 2020)

In the present work, nanoparticles of tin oxide (SnO<sub>2</sub>) annealed at temperatures of 400 °C, 500 °C, and 600 °C were prepared via solid-state reaction method. Structural and optical properties of prepared SnO<sub>2</sub> nanoparticles were analyzed by X-ray diffractometer (XRD), scanning electron microscope (SEM), elemental study was performed by energy-dispersive X-ray spectroscopy (EDAX), Fourier transform infrared spectroscopy (FTIR), dynamic light scattering (DLS) and ultraviolet-visible (UV-Vis) absorption characterizing techniques. The X-ray diffraction pattern confirms the pure tetragonal rutile structure of tin oxide nanoparticles without any impurity phase. SEM images depict the formation of nanorods at all annealing temperatures of 400 °C, 500 °C, and 600 °C while EDAX analysis confirms the presence of Sn and O without any impurities. UV-Vis absorption spectra show that the band gap of prepared tin oxide nanoparticles decreases initially from 3.44 eV at 400 °C to 3.03 eV at 500 °C and further increases to 3.39 eV at 600 °C. FTIR spectrum confirms the presence of O–Sn–O bond along with one unwanted absorption peak.

**Keywords:** Tin oxide, Nanoparticles, Temperature, Diffraction, Tetragonal.

DOI: [10.21272/jnep.12\(4\).04004](https://doi.org/10.21272/jnep.12(4).04004)

PACS numbers: 61.05.C, 61.82.Rx, 68.37.Hk, 82.20.Fw

### 1. INTRODUCTION

Tin oxide is one of the prominent transparent conducting oxides (TCOs) with excellent optical, electrical, and magnetic properties. It is an *n*-type semiconductor with a wide band gap [1]. Generally, tin oxide is found in two states: Stannous oxide (romarchite, SnO) and Stannic oxide (Cassiterite, SnO<sub>2</sub>), while the latter is more stable. The extraordinary optical, electrical, electrochemical properties and high surface to volume ratio of tin oxide nanoparticles ensure their applications in gas sensors [2, 3], antistatic coating [4], detection of combustible gases like H<sub>2</sub>S, CO, NO<sub>x</sub> and C<sub>2</sub>H<sub>5</sub>OH [5], dye-sensitized solar cells [6], optoelectronic devices [7], etc. Moreover, due to antimicrobial, antifungal, antiviral properties of tin oxide nanoparticles, it can be used for biomedical purposes, viz bone grafting, dental implants, in standard water filter and ultra-pure water filter [8].

Tin oxide nanoparticles can be synthesized by a number of the popular methods like sol-gel, high-energy ball milling, spray pyrolysis, hydrothermal, plasma process, solid-state reaction method, direct strike precipitation, aerosol flame deposition, solvothermal, polymerizing-complexing sol-gel method, polyol, oxidation, one step solid-state synthesis, molten salt, etc. [1, 9-12]. A literature survey confirms the formation of various shapes of tin oxide nanoparticles like a hollow sphere, spherical, nanotubes, nanotriangles, nanorods, wormholes, and many others [13]. Kim et al. [14] used thermal evaporation method for the preparation of tin oxide

nanoparticles, which have a size between 0.2 to 1.3 μm. Simin et al. [15] synthesized tin oxide nanoparticles via co-precipitation method (low-cost chemical method), and they possessed a tetragonal structure with spherical morphology. Luhua Jiang et al. [16] prepared tin oxide nanoparticles by heating ethylene glycol solutions containing SnCl<sub>2</sub> under atmospheric pressure. R. Rahmi and F. Kurniawan [17] used a high-voltage electrolysis method to synthesize tin oxide nanoparticles and they reported the average size distribution of nanoparticles in the range of 25-150 nm.

A tetragonal phase of tin oxides nanoparticles was prepared by M. Aziz et al. via sol-gel method using SnCl<sub>2</sub>·2H<sub>2</sub>O and polyethylene glycol at different calcination temperatures [18]. They found a relationship between the particle size, molecular weight of polyethylene glycol and temperature. The size of nanoparticles reduces if we decrease the calcination temperature while the molecular weight of polyethylene glycol increases. Kundu et al. [19] also used the same technique (sol-gel) and observed that the synthesized tin oxide nanoparticles are crystalline, agglomerated, and non-spherical while the annealed tin oxide nanoparticles are again crystalline. Ashok et al. [20] investigated the structural, morphological and optical properties of tin oxide nanopowders synthesized by the sol-gel technique. A.S. Ahmed et al. [21] prepared nanocrystalline tin oxide powders through a wet chemical route using tin metal as a precursor at different temperatures 300 °C,

\*drvvgarg78@gmail.com

500 °C, and 700 °C. They concluded that the structural properties of tin oxide nanoparticles mainly depend on lattice strain. They also found that the band gap reduces with an increase in sintering temperature. In the current work, we have investigated the structural, morphological and optical properties of tin oxide nanoparticles prepared by the solid-state reaction method at different annealing temperatures. This method has various advantages when compared with other methods as it is easy to handle, eco-friendly, high yield powder can be achieved in single synthesis, etc.

## 2. EXPERIMENTAL

### 2.1 Materials and Method

Tin oxides (SnO<sub>2</sub>) nanoparticles were prepared by a traditional solid-state reaction method. It is the simplest among all synthesis routes and requires less time for the formation of nanoparticles. Initially, we took commercially available powders of SnCl<sub>2</sub>·2H<sub>2</sub>O (4.52 g, 20 mMol) and NaOH (0.16 g, 40 mMol) and grinded both in a mortar pestle for 15 min and then mixed with NaCl (10.00 g) in a molar ratio of 1:2, respectively. All used chemicals were of AR grade. After that, we again crushed this mixture in a mortar pestle for another 30 min. The final mixture was oxidized and grown into tin oxide at different annealing temperatures 400 °C, 500 °C, and 600 °C in a furnace for 2 h. This experimental procedure results in the high-yield synthesis of tin oxide nanoparticles. Rod-shaped tin oxide nanoparticles were seen in SEM images with 98 % pure phase of tin oxide nanoparticles.

### 2.2 Characterizations

The purity of the sample, phase identification, and crystalline structure were studied in 2 $\theta$  scanning range of 20° to 90° by Rigaku Benchtop Powder X-ray diffractometer (monochromatic Cu-K $\alpha$  radiation,  $\lambda = 0.15408$  nm). Surface morphology and elemental analysis were analyzed by scanning electron microscope (SEM, model Zeiss EVOMA 10) and energy-dispersive X-ray spectroscopy (EDAX, model Oxford INCA 250). Dynamic light scattering (DLS) for particle size analysis was done by Malvern instruments nano series Zetasizer Nano-S. The optical properties and band gap studies were performed by the UV-2401 PC, UV-Vis spectrophotometer Shimadzu Corporation, Japan. Fourier transform infrared spectroscopy (FTIR) was used for the analysis of bond nature in all samples in the wave number range 4000-400 cm<sup>-1</sup> by FTIR spectrometer, Perkin Elmer, spectrum two model.

## 3. RESULTS AND DISCUSSION

### 3.1 Structural Analysis

Fig. 1 shows the X-ray diffraction (XRD) pattern of prepared tin oxide nanoparticles at different annealing temperatures 400 °C, 500 °C and 600 °C, respectively. The main diffraction peaks were observed at 27.3°, 31.70°, 34.1°, 45.5°, 51.9°, 56.5°, 66.2°, 75.3°, and 84.0° angles for (110), (200), (101), (210), (211), (002), (301), (202), and (410) planes, respectively. The XRD pattern obtained for tin oxide nanoparticles matches with the

JCPDS card no. 41-1445 [22]. XRD study confirms the polycrystalline nature and tetragonal rutile structure for all prepared tin oxide nanoparticles. Highest intensity peaks were observed at (200) plane for prepared tin oxide nanoparticles, which were annealed at temperatures 400 °C, 500 °C, and 600 °C, respectively, and no shift in peaks was observed. The average particle size ( $D$ , nm) for all samples prepared at different temperatures was calculated by Debye-Scherrer formula given by [23]:

$$D = \frac{0.9\lambda}{\beta \cos \theta}, \quad (1)$$

where  $D$  is the size of a particle;  $\lambda$  is the wavelength of light used, which is equal to 0.15408 nm;  $\beta$  is a full width half maximum (FWHM) of the corresponding peak and  $\theta$  is a diffracting angle. The average particle size was found to be of the order of 34.28 nm, 36.68 nm and 40.82 nm at 400 °C, 500 °C, and 600 °C, respectively. The average lattice parameters for prepared samples were found to be  $a = b = 4.7458$  and  $c = 3.1843$ . It was observed that with the rise in annealing temperature the size of the nanoparticles increases due to the diffusion of atoms from the grain boundary to the grain [24] which is more at the higher annealing temperature. Actually, at low annealing temperatures, the nanoparticles were regularly shaped, the granularity was uniform and slight agglomeration was seen, while at high annealing temperatures dense agglomerations were observed along with the irregular particle shape [25]. The stress vs strain ratio was also calculated for these nanoparticles prepared at different annealing temperatures and it was found to be 0.00136, 0.00740 and 0.00108, respectively.

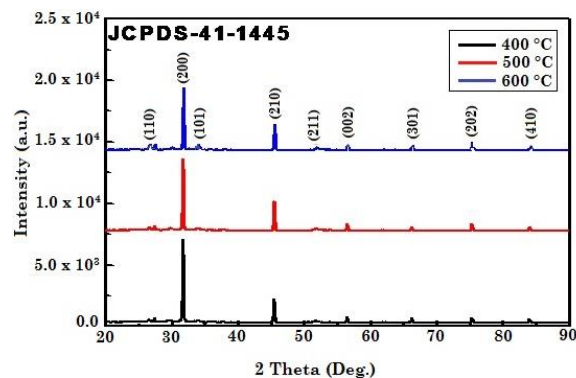


Fig. 1 – XRD patterns for dispersed SnO<sub>2</sub> nanoparticles in ethanol

### 3.2 SEM and EDAX Analyses

Fig. 2 shows the SEM images of tin oxide nanoparticles prepared by the solid-state reaction method annealed at temperatures 400 °C, 500 °C, and 600 °C, respectively. Fig. 2a shows clear visible nanoparticles having a spherical morphology along with a rod structure at 400 °C. Fig. 2b depicts the distributed spherical morphology of large size due to the agglomeration of particles, and some fine nanorods are also visible at 500 °C. Fig. 2c shows uniform spherical morphology along with the nanorods at 600 °C. It was also observed that with the rise of annealing temperature, particularly at 600 °C, grain size modified due to the overlapping

of grain boundaries. The analysis done by Image J software showed (on an average) the rod length and the area of tin oxide of 15.5 nm and 0.47 nm, respectively. The distribution and agglomeration enhanced with the annealing temperature. Thus, it is in good agreement with the above-mentioned analysis. Calculation done by Image J software is shown in Table 1.

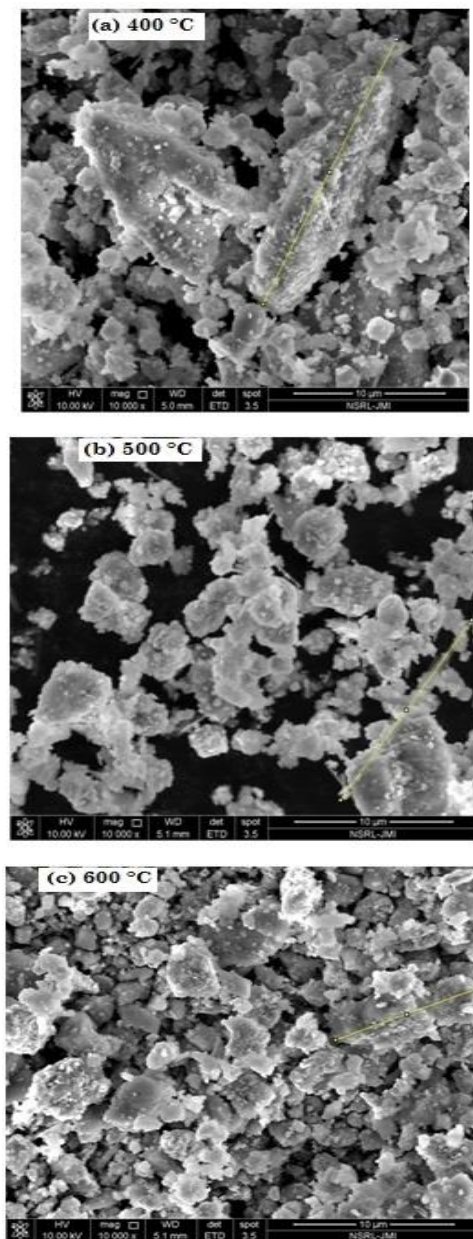


Fig. 2 – SEM images for dispersed SnO<sub>2</sub> nanoparticles in ethanol at (a) 400 °C, (b) 500 °C, and (c) 600 °C

Fig. 3 shows the EDAX spectra for tin oxide nanoparticles annealed at temperatures 400 °C, 500 °C, and 600 °C. The elemental analysis supports the presence of Sn and O and the absence of any kind of impurities in prepared powder samples. Thus, the purity of the samples can be examined with the supportive data received by EDAX spectral analysis of all the prepared samples annealed at different temperatures. The atomic percentage of Sn and O in prepared tin oxide nanoparticles is shown in Table 2.

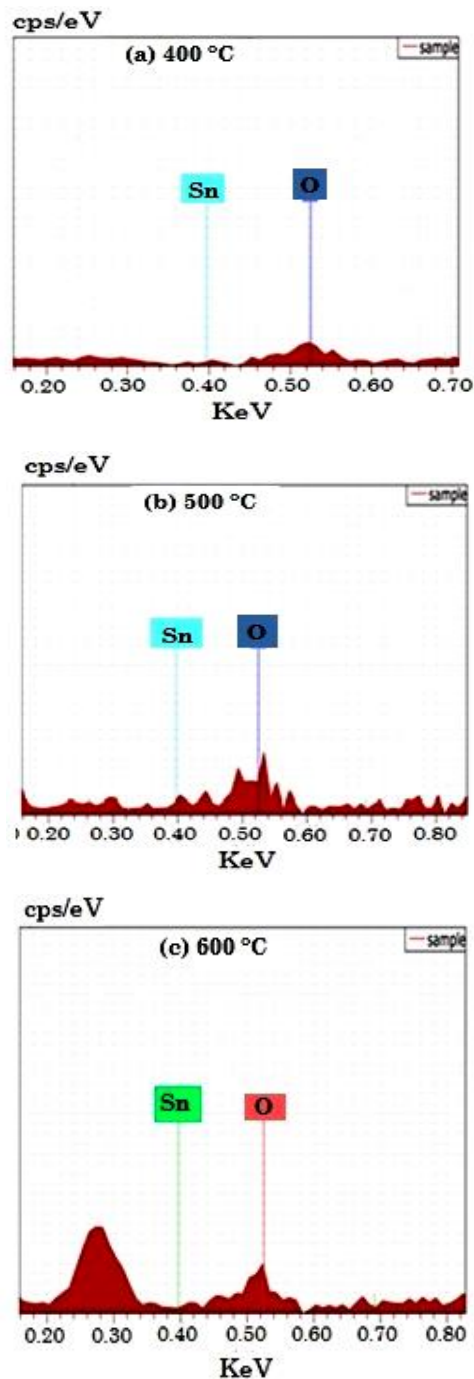


Fig. 3 – EDAX for dispersed SnO<sub>2</sub> nanoparticles in ethanol

Table 1 – Surface morphological parameters calculated by Image J software for dispersed SnO<sub>2</sub> nanoparticles in ethanol

Label	Area	Mean	Min.	Max.	Angle	Circ.	AR	Round	Solidity	Length
400 °C	0.63	124	68	213	64	0	0	0	0	21
500 °C	0.47	147	74	199	56	0	0	0	0	15
600 °C	0.31	126	78	248	23	0	0	0	0	10
	0.47									15.3

Table 2 – Atomic percentage for dispersed SnO<sub>2</sub> nanoparticles in ethanol

Elements	Atomic percentage at		
	400 °C	500 °C	600 °C
Sn	14.60	69.81	21.01
O	85.40	30.19	78.99

### 3.3 UV-Visible Spectroscopy

Fig. 4 shows the UV-Vis absorption spectra for tin oxide nanoparticles prepared by the solid-state reaction method at different annealing temperatures 400 °C, 500 °C, and 600 °C, respectively. The analyses of absorption spectra are one of the important tools with the help of which we can calculate the band gap of the prepared samples. It was observed from Fig. 4 that the nanoparticles annealed at 500 °C show high absorption and absorption decreases at 600 °C. In the visible region, high absorption occurs and no absorption is found in the UV region. The band gap for prepared nanoparticles was calculated by using the relation [10]:

$$(\alpha h\nu)^2 = (h\nu - E_g)^n, \quad (2)$$

where  $A$  is a constant,  $h$  is the Planck constant,  $\nu$  is the frequency,  $E_g$  is the band gap,  $\alpha$  is the absorption coefficient and the exponent  $n$  denotes the type of transition,  $n = 1/2$  for allowed direct,  $n = 2$  for allowed indirect,  $n = 3/2$  for forbidden direct and  $n = 3$  for forbidden indirect transitions, respectively. Fig. 5 shows a graph between  $(\alpha h\nu)^2$  and  $h\nu$ , the extrapolation of the curve along the  $x$ -axis gives  $E_g = 3.44$  eV at 400 °C,  $E_g = 3.03$  eV at 500 °C,  $E_g = 3.39$  eV at 600 °C. It has been observed that with the rise of annealing temperature from 400 °C to 500 °C the band gap ( $E_g$ ) decreases mainly due to two reasons. First, due to the decrease in carrier concentration and second, owing to the presence of empty states of the electronic states near the conduction band of the tin oxide lattice. Such variation in the optical band gap of degenerate semiconductors may be easily explained by the B-M effect [26]. As annealing temperature increases from 500 °C to 600 °C the absorption peak is shifted towards lower wavelengths due to which the band gap increases because of the quantum confinement effect [20].

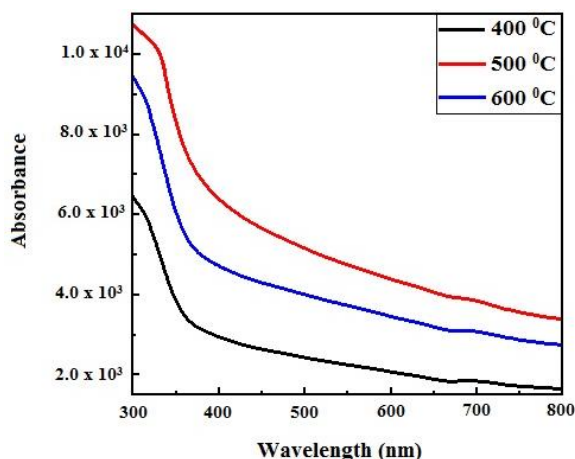


Fig. 4 – UV-Vis absorbance spectra for dispersed SnO<sub>2</sub> nanoparticles in ethanol

### 3.4 FTIR Spectrum

Fig. 6 depicts the FTIR spectrum for tin oxide nanoparticles annealed at different temperatures 400 °C, 500 °C, and 600 °C in the wavenumber region 4000-

400 cm<sup>-1</sup>. The strong absorption peaks available at 2975.52 cm<sup>-1</sup> and 1350.15 cm<sup>-1</sup> attribute to symmetric and asymmetric stretching vibrations of –CH<sub>2</sub> and –CH<sub>3</sub> groups [24]. The strong absorption peak at 1628.50 cm<sup>-1</sup> attributes to the H–O–H bond from water molecules present in the atmosphere. Some sharper absorption peaks are also visible in the spectrum at 623.11 cm<sup>-1</sup> and 573.01 cm<sup>-1</sup> [27]. The absorption peak at 623.11 cm<sup>-1</sup> corresponds to the stretching vibration of the O–Sn–O bond and there is one unwanted peak at 573.01 cm<sup>-1</sup> which may have originated due to crystal lattice defects or disorder because of the lattice dislocation [28-30].

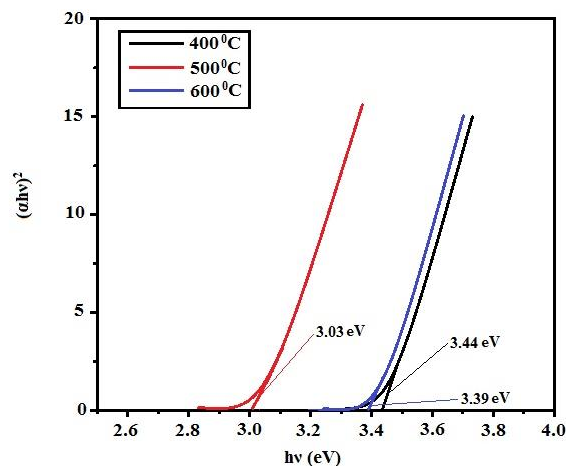


Fig. 5 – Tauc plot for dispersed SnO<sub>2</sub> nanoparticles in ethanol

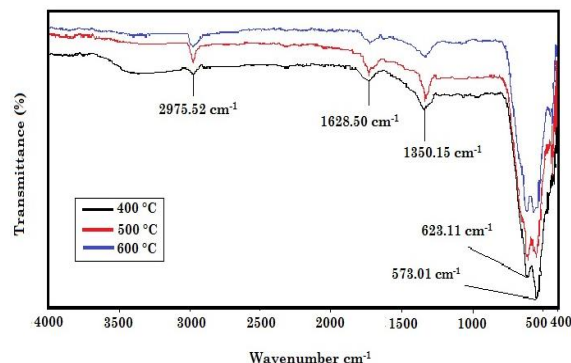


Fig. 6 – FTIR spectrum for dispersed SnO<sub>2</sub> nanoparticles in ethanol

### 3.5 Dynamic Light Scattering (DLS) Analysis

Fig. 7 and Fig. 8 depict the hydrodynamic diameter and correlation coefficient of the dispersed tin oxide nanoparticles in ethanol by dynamic light scattering (DLS) which is found to be in supportive results similar to XRD in terms of particle size (in the range of 30 nm). The correlation coefficient shows that the absorption wavelength is similar to all the samples annealed at temperatures 400 °C, 500 °C, and 600 °C. Thus, its polydispersity percentage is 61.7 % and its polydispersity index is 0.38 when dispersed in ethanol for analysis i.e., all three samples of tin oxide have almost the same particle sizes.

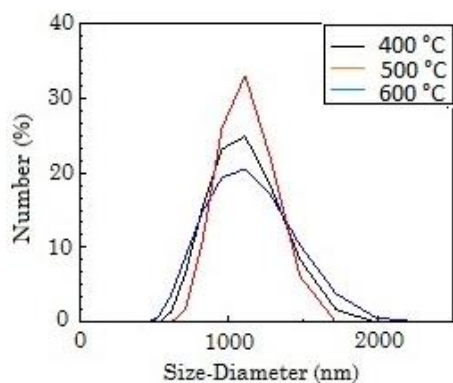


Fig. 7 – The hydrodynamic diameter of the dispersed SnO<sub>2</sub> nanoparticles in ethanol by DLS

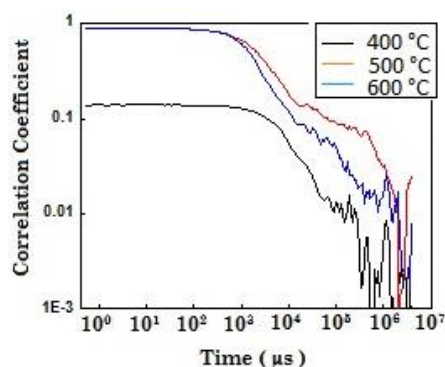


Fig. 8 – The correlation coefficient of the dispersed SnO<sub>2</sub> nanoparticles in ethanol by DLS

#### 4. CONCLUSIONS

Tin oxide nanoparticles were prepared by the solid-state reaction method. XRD patterns support the polycrystalline nature and tetragonal rutile structure of these nanoparticles. The calculated average particle size

was observed to be in ascending order along with the increase in temperature and it varied from 34.28 nm to 40.82 nm for different annealing temperatures 400 °C, 500 °C to 600 °C, and it has been found that the crystallinity of prepared samples enhanced. SEM images confirm the formation of a rod-like structure along with the spherical morphology of nanoparticles. The formation of unadulterated tin oxide nanopowder was validated by EDAX analysis. The energy band gap of tin oxide nanoparticles decreases with increase in temperature from 400 °C to 500 °C due to a decrease in carrier concentration and due to the presence of unfilled electronic states near the conduction band of the tin oxide lattice while the band gap increases with an increase in temperature from 500 °C to 600 °C due to quantum confinement effect. Besides, the band gap ( $E_g$ ) of tin oxide nanoparticles depends on lattice strain. Thus, we conclude that the optical properties of the tin oxide nanoparticles can be modulated by varying the annealing temperature. FTIR spectrum confirms the formation of tin oxide nanoparticles. Therefore, the solid-state reaction method offers a simple route for the preparation of spherical shape tin oxide nanoparticles along with its nanorods. It was observed that the nanoparticles annealed at 500 °C have good optical properties which makes them suitable for gas sensor applications.

#### ACKNOWLEDGEMENTS

One of the authors Vijay Garg is highly thankful to CST U.P., Lucknow for providing financial assistance via letter no. CST/D-726 dated 09/06/2016. The author is feeling obliged to Prof. R.C. Lal, Principal M.M. College Modinagar for giving the necessary support and infrastructure in college to complete this work and project. The authors would like to acknowledge Dr. D.K Aswal, Director CSIR-NPL, India, for supporting the research work and providing the necessary characterization facilities.

#### REFERENCES

- M.A. Farrukh, H.B. Teck, R. Adnan, *Turk. J. Chem.* **34**, 537 (2010).
- A.R. Phani, S. Manorama, V. Rao, *J. Mater. Chem. Phys.* **58**, 101 (1999).
- A.R. Phani, S. Manorama, V.J. Rao, *J. Phys. Chem. Solids* **61** No 6, 985 (2000).
- Y.-S. Cho, G.-R. Yi, J.-J. Hong, S.H. Jang, S.-M. Yang, *Thin Solid Films* **515** No 4, 1864 (2006).
- K.-W. Kim, P.-S. Cho, S.-J. Kim, J.-H. Lee, C.-Y. Kang, J.-S. Kim, S.-J. Yoon, *Sensor. Actuat. B* **123** No 1, 318 (2007).
- H. Chae, D. Song, Y.-G. Lee, T. Son, W. Cho, Y.B. Pyun, T.-Y. Kim, J.-H. Jee, F. Fabregat-Santiago, J. Bisquert, Y.S. Kang, *J. Phys. Chem. C* **118** No 30, 16510 (2014).
- J.H. He, T.H. Wu, C.L. Hsin, K. Li, L.J. Chen, Y.L. Chueh, L.J. Chou, Z. Wang, *Small* **2** No 1, 116 (2006).
- S.M. Amininezhad, A. Rezvani, M. Amouheidari, S.M. Amininejad, S. Rakhshani, Zahedan, *J. Res. Med. Sci.* **17** No 9, e1053 (2015).
- M.-M. Bagheri-Mohagheghi, N. Shahtahmasebi, M.R. Alinejad, A. Youssefi, M. Shokoooh-Saremi, *Physica B* **403** No 13-16, 2431 (2008).
- R. Khanom, M.A.A. Khan, A. Gafur, S. Akter, S. Ahmed, M. Shahjahan, M.R. Qadir, *Nanoscience and Nanometrology* **3** No 1, 12 (2017).
- Y. Kim, Y. Yoon, D. Shin, *J. Ceram. Process. Res.* **11** No 6, 673 (2010).
- Y. Wang, J.Y. Lee, *J. Phys. Chem. B* **108** No 46, 17832 (2004).
- H.X. Yang, J.F. Qian, Z.X. Chen, X.P. Ai, Y.L. Cao, *J. Phys. Chem. C* **111** No 38, 14067 (2007).
- H.W. Kim, S.H. Shim, C. Lee, *Ceram. Int.* **32** No 8, 943 (2006).
- S. Tazikheh, A. Akbari, A. Talebi, E. Talebi, *Mater. Sci-Poland* **32** No 1, 98 (2014).
- L. Jiang, G. Sun, Z. Zhou, S. Sun, Q. Wang, S. Yan, H. Li, J. Tian, J. Guo, B. Zhou, Q. Xin, *J. Phys. Chem. B* **109** No 18, 8774 (2005).
- R. Rahmi, F. Kurniawan, *Bull. Chem. React. Eng. Catal.* **12** No 2, 281 (2017).
- M. Aziz, S.S. Abbas, W.R.W. Baharom, *Mater. Lett.* **91**, 31 (2013).
- V.S. Kundu, R.L. Dhiman, D. Singh, A.S. Maan, S. Arora, *Int. J. Adv. Res. Sci. Eng.* **2**, 21 (2013).
- A.D. Bhagwat, S.S. Sawant, B.G. Ankamwar, C.M. Mahajan, *J. Nano-Electron. Phys.* **7** No 4, 04037 (2015).
- A.S. Ahmed, A. Azam, S.M. Muhamed, M. Chaman, S. Tabassum, *J. Phys. Chem. Solids* **73** No 7, 943 (2012).
- Z. Yang, G. Du, Z. Guo, X. Yu, S. Li, Z. Chen, P. Zhang, H. Liu, *Nanoscale* **2**, 1011 (2010).
- P. Nirmal Prashanth, P. Rajesh, R. Ramasamy, V. Vijayan, *Optik* **135**, 434 (2017).
- P. Chetri, A. Choudhary, *Physica E* **47**, 257 (2013).

25. S. Gao, L. Pang, H. Che, X. Zhou, *China Particuology* 2 No 4, 177 (2004).
26. A. Ayeshamariam, S. Ramalingam, M. Bououdina, M. Jayachandran, *Spectrochim. Acta A* 118, 1135 (2014).
27. M. Salavati-Niasari, N. Mir, F. Davar, *Inorg. Chim. Acta* 363 No 8, 1719 (2010).
28. J. Chen, J. Wang, F. Zhang, D. Yan, G. Zhang, R. Zhuo, P. Yan, *J. Phys. D: Appl. Phys.* 41 No 10, 105306 (2008).
29. S. Chacko, N.S. Philip, K.G. Gopchandran, P. Koshy, V.K. Vaidyan, *Appl. Surf. Sci.* 254 No 7, 2179 (2008).
30. A. Dieguez, A. Romano-Rodriguez, A. Vila, J.R. Morante, *J. Apl. Phys.* 90, 1550 (2001).

## Синтез та характеристика температурно-контрольованих наночастинок SnO<sub>2</sub>, виготовлених методом твердої реакції

Vijay Garg<sup>1</sup>, Harsh Sharma<sup>1</sup>, Divya Rehani<sup>2,3</sup>, Renu Kumari<sup>2,4</sup>, Vipin Kumar<sup>4</sup>, Manoj Kumar Tiwari<sup>5</sup>, Shailesh Narain Sharma<sup>3,6</sup>, Manish Saxena<sup>7</sup>

<sup>1</sup> Department of Physics, M.M. College Modinagar, Ghaziabad (U.P) 201204, India

<sup>2</sup> Dr. A.P.J. Abdul Kalam Technical University, Lucknow (U.P.) 226031, India

<sup>3</sup> Council of Scientific & Industrial Research-National Physical Laboratory, New Delhi 110012, India

<sup>4</sup> Department of Physics, KIET Group of Institutions, Ghaziabad (U.P.) 201206, India

<sup>5</sup> Department of Electronics, Bhaskaracharya College of Applied Science, Delhi University, Delhi 110075, India

<sup>6</sup> Academy of Scientific and Innovative Research ACSIR, Ghaziabad (U.P.) 201002, India

<sup>7</sup> Moradabad Institute of Technology, Moradabad 244001, India

У роботі наночастинок оксиду олова (SnO<sub>2</sub>), відпалені при температурах 400, 500 та 600 °C, були підготовлені методом твердої реакції. Структурні та оптичні властивості підготовлених наночастинок SnO<sub>2</sub> аналізували за допомогою рентгенівського дифрактометра (XRD) та скануючого електронного мікроскопа (SEM). Елементне дослідження було виконано енергетично-дисперсійною рентгенівською спектроскопією (EDAX), інфрачервоною спектроскопією з використанням перетворення Фур'є (FTIR), методами динамічного розсіювання світла (DLS) та поглинання світла в ультрафіолетовому та видимому діапазонах (UV-Vis). Рентгенівська дифрактограма підтверджує чисту тетрагональну структуру рутилу наночастинок SnO<sub>2</sub> без будь-якої домішкової фази. SEM зображення відображають утворення нанострижнів при всіх температурах відпалу 400, 500 і 600 °C, тоді як EDAX аналіз підтверджує наявність Sn і O без будь-яких домішок. UV-Vis спектри показують, що ширина забороненої зони підготовлених наночастинок SnO<sub>2</sub> спочатку зменшується з 3,44 eV при температурі 400 °C до 3,03 eV при 500 °C, а потім збільшується до 3,39 eV при температурі 600 °C. Спектр FTIR підтверджує наявність зв'язку O–Sn–O разом з одним небажаним піком поглинання.

**Ключові слова:** Оксид олова, Наночастинок, Температура, Дифракція, Тетрагональний.